IEICE TRANS. COMMUN., VOL.E94–B, NO.7 JULY 2011

INVITED PAPER *Joint Special Section on Opto-electronics and Communications for Future Optical Network*

Synchronous Demodulation of Coherent 16-QAM with Feedforward Carrier Recovery

Ali AL-BERMANI[†a)], **Christian WÖRDEHOFF**[††b)], **Sebastian HOFFMANN**[†c)], **Timo PFAU**[†*], **Ulrich RÜCKERT**[††], ***and*** **Reinhold NOÉ**[†], ***Nonmembers***

SUMMARY We present the recovery of 2.5 Gb/s synchronous 16-point quadrature amplitude modulation data in real-time for an linewidth-times-symbol-duration ratio of 0.00048 after transmission over 1.6 km standard single mode fiber.

key words: *optical communication, 16ary quadrature amplitude modulation, coherent communication, phase estimation, feedforward carrier recovery*

1. Introduction

Coherent optical transmission allows for improved bandwidth utilization and impairment compensation of existing optical fiber links and is a key for future communication systems with transmission rates of 112 Gb/s and above. In recent years quadrature phase shift keying (QPSK) was the preferred modulation format because of its robustness on long-haul links [1]–[3]. However, for metropolitan area networks, higher-order quadrature amplitude modulation is permissible namely 16-QAM, which doubles spectral efficiency. Simulations and offline experiments have recently been published [4]–[10], but real-time investigations are essential for progress towards commercial applications [11], [12]. Field programmable gate arrays (FPGA) enable evaluating digital receiver algorithms in real-time experiments before being implemented as CMOS circuits.

Within this paper, we present a 2.5 Gb/s real-time 16-QAM transmission experiment with FPGA-based digital signal processing (DSP) that contains our phase noise tolerant QAM carrier recovery algorithm [13]. This paper is organized as follows:

Section 2 explains the general principles of 16-QAM transmission and coherent detection. Coherent transmission is usually employed for all higher modulation formats because it delivers magnitude and phase information to the electronic part of the receiver. An important element of the digital receiver is the phase estimator also referred to as intermediate frequency (IF) carrier recovery which is described in detail within Sect. 3. The phase estimator works in a feedforward structure which allows data recovery based on an estimation not delayed by a feedback loop. Section 4 describes the experimental setup, and Sect. 5 presents and discusses the measurement results.

2. Coherent 16-QAM Transmission

16-QAM modulation combined with polarization multiplex (PM) doubles the capacity of existing PM-QPSK transmission systems, as shown in Fig. 1, but requires transmitters and receivers with increased complexity. The following subsections describe the general implementation strategies for both.

2.1 16-QAM Transmitter

There are several possible implementations for an optical square 16-QAM transmitter [14], [15]. The common structures are presented in Fig. 2. The serial square 16-QAM transmitter contains a Mach-Zehnder modulator (MZM) and a phase modulator (PM) in series shown in Fig. 2(a). This structure features a simple optical part, but phase modulation requires a 12-ary electrical driving signal. High-speed digital-to-analog converters (DAC) with high-resolution are required to perform electro-optical (E/O) interfacing. Using separate serial structures for I and Q modulation displayed in Fig. 2(b) leads to a higher optical complexity and necessitating integration, but allows binary input levels. Phase modulators in the 16-QAM transmitter structure temporarily yield to high optical power, where phasors with amplitudes

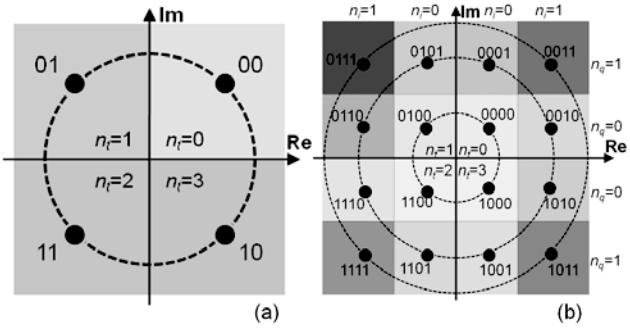

Fig. 1 QPSK (a) and square 16-QAM (b) constellation diagrams.

Manuscript received December 23, 2010.
Manuscript revised March 3, 2011.

[†]The authors are with Optical Communication and High-Frequency Engineering, University of Paderborn, EIM-E, Warburger Str. 100, D-33098 Paderborn, Germany.
[††]The authors are with the Center of Excellence - Cognitive Interaction Technology CITEC, Bielefeld University, D-33165 Bielefeld, Germany.
[*]Presently, with Alcatel-Lucent, Murray Hill, USA.
a) E-mail: albermani@ont.upb.de.
b) E-mail: cwoerdeh@cit-ec.uni-bielefeld.de
c) E-mail: sebastian.hoffmann@uni-paderborn.de

DOI: 10.1587/transcom.E94.B.1794

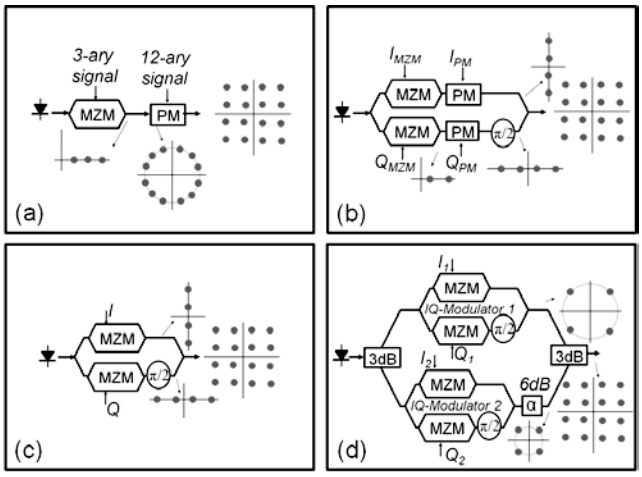

Fig. 2 Optical square 16-QAM transmitters; serial MZM with PM(a), IQ-setup with MZM and PM (b), conventional IQ setup (c), and quad-parallel MZM setup (d).

greater than one are possible during the symbol transitions [14]. In contrast pure IQ transmitters shown in Fig. 2(c) are composed of two arms, leading also to a bigger optical complexity, but the electrical driving signals manage with four levels. Combining two IQ transmitters to a quad-parallel MZM proposed in [15] and presented in Fig. 2(d) allows again binary driving signals at the costs of the highest optical complexity of all four structures but provides the best performance for high baud rates with respect to E/O interfacing. In pure IQ transmitters there will be symbol transitions through zero in the constellation diagrams. If we consider chirp, the best transmission setup will be equipped with a conventional IQ transmitter, where chirp and normalized intensity is comparatively small. The chirp characteristic of the other transmitters is more disadvantageous because chirp appears simultaneously with high power levels. For that reason the common IQ transmitter is used in our experiments.

2.2 Coherent Receiver

Coherent receivers usually consist of a frontend with polarization diversity, optical 90° hybrids, O/E conversion, analog-to-digital converters (ADCs) and a digital signal processing unit (DSPU). ADCs and DSPU will be integrated in a single chip to ease interfacing, reduce footprint size and energy consumption. Field programmable gate arrays (FPGAs) can be employed to verify and evaluate DSP algorithms in realtime experiments, but they are insufficient for commercial implementation in terms of available performance and energy efficiency.

Figure 3 shows a simplified block diagram of an optical transmission system with coherent detection and polarization multiplex. The intradyne receiver signal is produced by an unmodulated LO laser and two 90° hybrids for the optical demodulation and separation. After photodetection, in-phase and quadrature (I&Q) portions of the electric fields

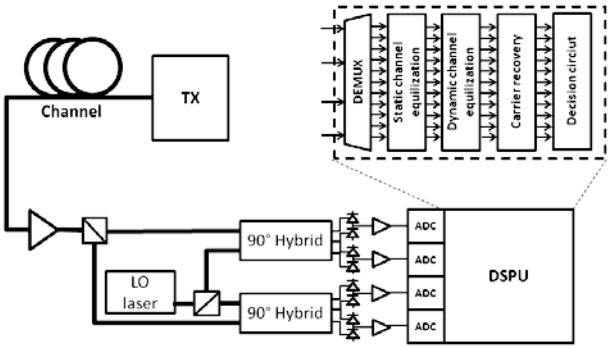

Fig. 3 Simplified block diagram of an optical transmission system with coherent detection and digital signal processing.

are sampled by the ADCs and fed into the DSPU.

The DSPU contains several subsystems to overcome static and dynamic channel impairments as well as laser phase noise and inadequate receiver setups in the digital domain [16]. After CD equalization and clock recovery PMD can be compensated within separating both polarizations. Frequency and phase estimations are performed on both channels before the transmitted symbols are finally decoded. High baud rates of optical transmission links require M-fold parallelization of the digital signal processing to meet technology parameters. This results in several constraints for algorithm structure and computational complexity [11].

3. Feedforward Carrier Recovery

Even the unmodulated IF signal contains phase noise corresponding to the sum linewidth of TX and LO lasers. If there is no automatic LO frequency control the IF generally differs from zero. A non-zero IF leads to a deterministic phase slope on adjacent samples which can be employed for frequency estimation [17]. The random phase noise has to be tracked by a phase estimation stage that also removes residual frequency offsets due to imperfect frequency estimation or LO frequency control. The effort for phase estimation (calculation of a time series of angles, real numbers within a limited range) depends on the modulation format.

For star constellations (BPSK, QPSK, 8-PSK and certain QAM formats) it is obviously advantageous to convert the received symbols to polar coordinates and to demodulate them by a simple subtraction of signal and carrier phase angles [18]. In contrast, the more common square constellation QAM formats require a rotation in the complex plane for demodulation, to adjust them to non-radial decision boundaries. Feedforward phase estimators (PE) using the QPSK Partitioning scheme [19], [20], require less computational effort in comparison to minimum distance PE concepts [21], [22], but are more sensitive against noise effects, especially for higher order QAM constellations. Due to the laser linewidth tolerance and limited computational resources, [13] was chosen for this experiment. The algorithm and its implementation is described in the following subsections.

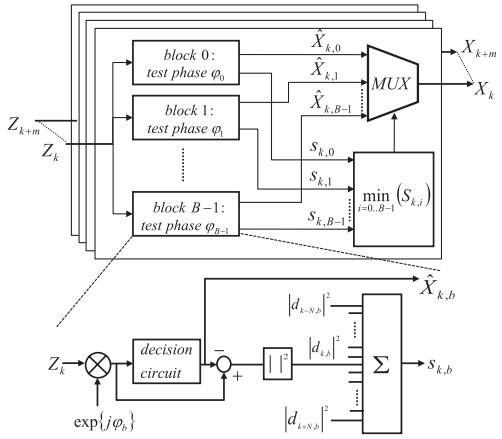

Fig. 4 Feedforward recovery using B test phase values φ_b. (© 2009 IEEE)

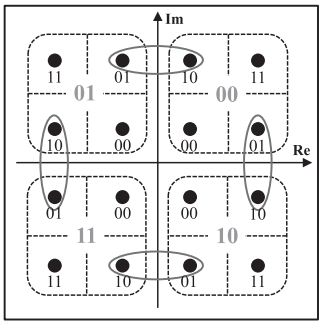

Fig. 5 Partial differential encoding for a square 16-QAM constellation. (© 2009 IEEE)

3.1 Algorithm

Figure 4 shows a block diagram of the employed carrier recovery module. The input signal Z_k of the coherent receiver is sampled at the symbol rate. For the theoretical description perfect clock recovery and equalization are assumed [13]. In order to recover the carrier phase the received signal Z_k is rotated by B test carrier phase angles φ_b which are equally spaced:

$$\varphi_b = \frac{b}{B} \cdot \frac{\pi}{2}, \quad b \in \{0, 1, \ldots, B-1\}. \tag{1}$$

Afterwards, all rotated symbols are fed into a decision circuit and the squared distance $\left|d_{k,b}\right|^2$ to the closest constellation point is calculated in the complex plane:

$$\begin{aligned} \left|d_{k,b}\right|^2 &= \left|Z_k \exp\{j\varphi_b\} - \lfloor Z_k \exp\{j\varphi_b\} \rfloor_D\right|^2 \\ &= \left|Z_k \exp\{j\varphi_b\} - \hat{X}_{k,b}\right|^2 \end{aligned} \tag{2}$$

In order to reduce the influence of channel noise distortions, the distances of $2N + 1$ consecutive symbols rotated by the same carrier phase angle φ_b are summed up to a mean square error quantity $S_{k,b}$:

$$s_{k,b} = \sum_{n=-N}^{N} \left|d_{k-n,b}\right|^2 \tag{3}$$

The optimum value of the filter half width N depends on the laser linewidth times symbol rate product. $N = 6, \ldots, 10$ turned out to be a fairly good choice in simulation [13].

After filtering, the optimum phase angle is determined by searching the minimum sum of distance values. As the decoding was already executed in (2), the decoded output symbol $\hat{X}_k$ can be selected from the $\hat{X}_{k,b}$ by a switch controlled by the index $m_{k,min}$ of the minimum distance sum.

Due to the 4-fold ambiguity of the recovered phase in the square M-QAM constellation the first two bits which determine the quadrant of the complex plane should be differentially Gray-encoded. The differential encoding and decoding process is the same as for QPSK and is presented in detail in [23]. It can be described by the following formula

$$\begin{aligned} &n_{o,k} = \left(n_{r,k} - n_{r,k-1} + n_{j,k}\right) \bmod 4 \\ &n_{o,k}, n_{r,k}, n_{j,k} \in \{0, 1, 2, 3\} \end{aligned} \tag{4}$$

where $n_{o,k}$ is the differentially decoded quadrant number, $n_{r,k}$ is the received quadrant number and $n_{j,k}$ is the jump number. The only required modification of the decoding process compared to [23] is that quadrant jumps are detected according to the following formula:

$$n_{j,k} = \begin{cases} 1 & \text{if } m_{k,\min} - m_{k-1,\min} > M/2 \\ 3 & \text{if } m_{k,\min} - m_{k-1,\min} < -M/2 \\ 0 & \text{otherwise} \end{cases} \tag{5}$$

For all other bits that determine the symbol within the quadrant of the complex plane, normal Gray-coding is sufficient and no differential encoding/decoding is required. Figure 5 illustrates the bit to symbol assignment including differential encoding/decoding for square 16-QAM. The resulting constellation diagram is not any longer Gray-encoded. This multplies the BER by a factor of 2 for 4-QAM (QPSK), 1.67 for 16-QAM, and less (approaching 1) for high order QAM constellations [24].

3.2 Hardware Efficient Carrier Recovery Implementation

The rotation of a symbol in the complex plane normally requires a complex multiplication, consisting of four real-valued multiplications with subsequent summation. This would lead to a large number of multiplications to be executed, while achieving a sufficient resolution B for the carrier phase values φ_b. The hardware effort would therefore become prohibitive. Applying the CORDIC (coordinate rotation digital computer) algorithm [25] can dramatically reduce the necessary hardware effort to calculate the B rotated test symbols. This algorithm can compute vector rotations simply by summation and shift operations. As for the calculation of the B rotated copies of the input vector intermediate results can be reused for different rotation angles, the number of shift and add operations required to generate the B test symbols is given by

$$n_{op} = \sum_{b=1}^{\log_2 B} 2^{b+1} \tag{6}$$

For $B = 16$, the CORDIC algorithm requires only 60 shift and add operations whereas complex multiplication of Z_k with 16 test phasors would require 64 real multipliers and 32 adders. To determine the closest constellation point $\hat{X}_{k,b}$ the rotated symbols are fed into a decision circuit. The square distance (2) can be written as

$$\begin{aligned} \left|d_{k,b}\right|^2 &= (Re\left[d_{k,b}\right])^2 + (Im\left[d_{k,b}\right])^2 \\ &= \left(Re\left[Z_k \exp\{j\varphi_b\}\right] - Re\left[\hat{X}_{k,b}\right]\right)^2 \\ &\quad + \left(Im\left[Z_k \exp\{j\varphi_b\}\right] - Im\left[\hat{X}_{k,b}\right]\right)^2 \end{aligned} \tag{7}$$

Implementing this formula literally into hardware would lead to two multipliers and three adders, but a closer examination of (2) and (7) reveals that the results of the subtractions are relatively small because the distance to the closest constellation point is calculated. Therefore, the most significant bits (MSBs) of the subtraction result will always be zero and can be discarded to reduce the hardware effort. Due to the moderate resolution required for d^2, the squared distance (3) can be determined by a look-up table or basic logic functions more efficiently than by multipliers.

Parallel systems allow a very efficient implementation of the summation of $2N+1$ consecutive values. The adders can be arranged in a binary tree structure where intermediate results from different modules are reused in neighboring modules leading to a moderate hardware effort.

4. Experimental Setup

Figure 6 shows the experimental setup of an optical 2.5 Gbit/s realtime 16-QAM transmission system, based on our earlier QPSK transmission setup [1]. To resolve the fourfold ambiguity of the estimated optical phase within the receiver, the quadrant numbers of the in-phase (I) and quadrature (Q) data streams are modulo 4 differentially encoded, cf. Fig. 5. For 16-QAM data supply, two uncorrelated 625 Mbaud quaternary data streams are generated by an FPGA, modulator drivers, attenuators, and resistive summers. These drive a dual-parallel Mach-Zehnder modulator (DPMZM) consisting of two Mach-Zehnder interferometers, cf. Fig. 2(c). An external cavity laser (ECL) is employed in a self-homodyne arrangement (150 kHz specified linewidth, 1.5 dBm output power).

The ECL signal passes an Erbium-doped fiber amplifier (EDFA) and is split. One signal portion is fed into the DPMZM for transmission (TX) while the other portion replaces the local oscillator (LO) laser for coherent reception. Fiber launch power at the TX-EDFA output is −1.5 dBm. After transmission through 1.6 km of SMF, the signal is fed into a variable optical attenuator (VOA), followed by an EDFA and a ∼20 GHz wide bandpass filter for noise filtering. In Fig. 7 the optical signal before (a) and after (b) transmission is plotted, as measured in an oscilloscope at the marked positions in Fig. 6.

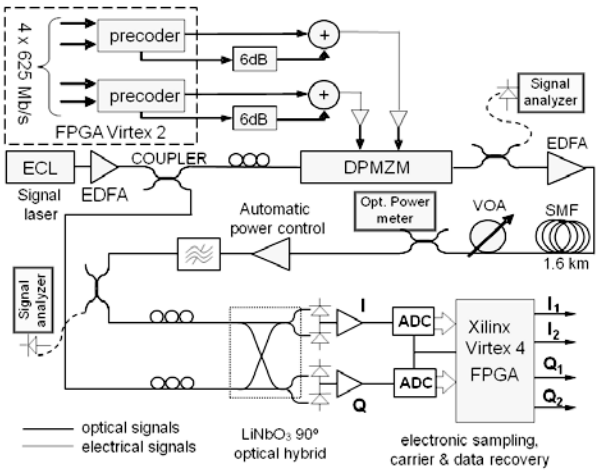

Fig. 6 16-QAM transmission setup with real-time synchronous coherent digital I&Q receiver.

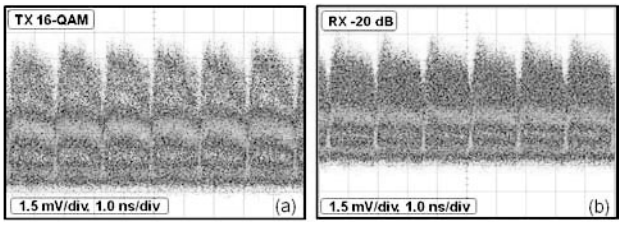

Fig. 7 Intensity patterns of 625 Mbaud 16-QAM after DPMZM (a), after 1,6 km for −20 dBm (b).

Polarization is controlled manually. TX and LO signals are superimposed in a $LiNbO_3$ 90° optical hybrid and detected in two differential photodiode pairs.

The electrical I&Q signal components are amplified before being sampled in two 6-bit analog-digital converters (ADCs) at the symbol rate of 625 MHz. The ADCs interface with a Xilinx Virtex 4 FPGA where carrier and data is recovered electronically.

The received input samples I and Q are combined as a symbol pointer in the complex plane. Signals are digitally processed in $M = 8$ demultiplexed parallel streams, thereby reducing the internal clock frequency to 78.125 MHz. As mentioned in Sect. 3 the carrier recovery does not contain any feedback loop, so it can be adapted to any transmission rate by increasing M. The optimum response halfwidth N of the squared-distance filter depends on the laser-sum-linewidth-times-symbol-interval-product; we chose $N = 6$ for this experiment, which worked best. For bit-error-ratio (BER) measurement, appropriate patterns are programmed into the BER tester.

While the hardware effort for carrier recovery is on the order of $B = 16$ times larger than for QPSK, capacity is all the same doubled.

The designed digital carrier recovery is performance constrained due to ADC resolution and linewidth-times-symbol-duration product values as it is presented in Fig. 8.

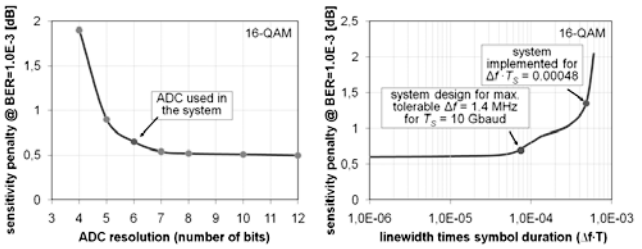

Fig. 8 Receiver sensitivity penalty vs. analog-to-digital converter resolution (left) and receiver tolerance against phase noise (right) for square16-QAM constellation.

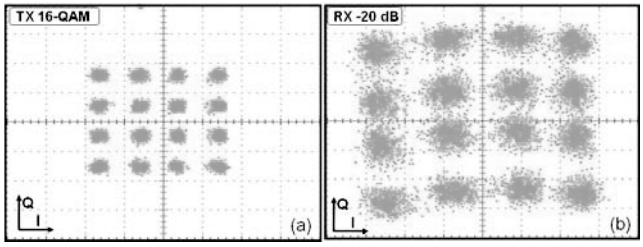

Fig. 9 16-QAM constellation in the transmitter (a) and after optical transmission for −20 dBm(b).

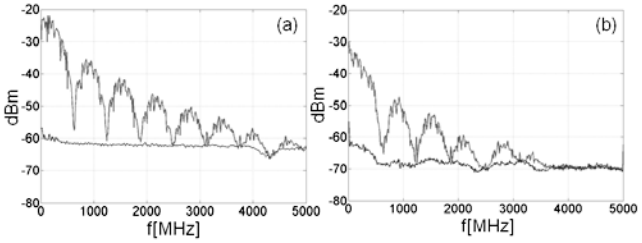

Fig. 10 Electrical spectra in one quadrature with either aligned (top) or orthogonal (bottom) polarizations, showing signal and noise, for −20 dBm (a) and −40 dBm (b) preamplifier input power.

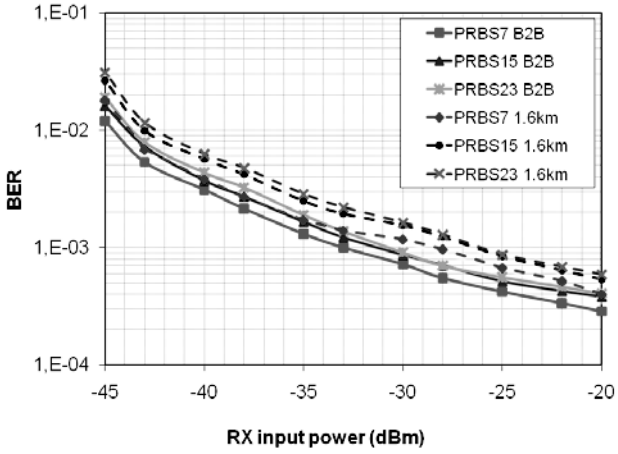

Fig. 11 Measured BER vs. optical power at the preamplifier input, averaged over all 4 subchannels (I1, Q1, I2 and Q2) at 2.5 Gbit/s data rate.

Based on simulation results, an effective converter resolution of at least 7 bit and a $\Delta f \cdot T \leq 10^{-4}$ is required for optimal performance. Limited resolution and sample rate of the employed ADCs result in a suboptimal operating point, which leads to an expected overall sensitivity penalty of 0.9 dB for a BER of 10^{-3} in simulation.

5. Measurement Results

Electrical 16-QAM data transmission was error-free. Figure 9 shows the electrical constellation diagram in the transmitter (a) and after optical transmission over 1.6 km of SMF for −20 dBm (b) preamplifier input power. Figure 9(b) shows severe distortion with high noise compared to Fig. 9(a), mainly due to the low ECL transmission power used (1.5 dBm). Two EDFAs and the high attenuation of the VOA also contribute to the noise. An SNR of 35 dB was measured at one ADC input, using electrical noise power in a 312.5 MHz band and total electrical signal power. Corresponding spectra are shown in Fig. 10.

Figure 11 shows the BER versus received power for 2.5 Gbit/s transmission back-to-back and over a distance of 1.6 km of SMF, using $2^7 - 1$, $2^{15} - 1$ and $2^{23} - 1$ PRBS data. The best measured BERs were at $2.85 \cdot 10^{-4}$ and $4 \cdot 10^{-4}$ for $2^7 - 1$, $3.8 \cdot 10^{-4}$ and $5.4 \cdot 10^{-4}$ for $2^{15} - 1$, and $4.05 \cdot 10^{-4}$ and $5.9 \cdot 10^{-4}$ for $2^{23} - 1$ PRBS data, for back-to-back and 1.6 km, respectively. All PRBS could be detected until the preamplifier input power was set below −45 dBm.

All measurements were repeated several times and turned out to be stable.

Figure 12 shows measured BERs versus preamplifier input power of all I&Q subchannels for various PRBS lengths over 1.6 km SMF. The curves are averaged over I&Q but separated for the inter-quadrant bits (IQ1) and intra-quadrant bits (IQ2) because of the different encoding methods.

Intra-quadrant decoding is limited more strongly than inter-quadrant decoding, presumably by intersymbol interference (ISI) in the non-ideal electrical transmitter. This is seen from the fact that the BER of I2 and Q2 (inside quadrant) is higher than the BER of the quadrant numbers I1 and Q1. Based on simulations without ISI we estimated the BER floor to be ideally at 10^{-4} for our $\Delta f \cdot T = 0.00048$. Averaged over all 4 subchannels (I1, Q1, I2 and Q2) at received powers larger than −30 dBm, the measured BER was all the same less than the forward-error corrections (FEC) limit ($2 \cdot 10^{-3}$). An appropriate FEC code (which was actually not employed within this experiment) would cause 7% overhead and decrease the net data rate. As mentioned above, $N = 6$ of the carrier recovery is optimum for a single-polarization 16-QAM system in our experimental setup. Note that with a higher received power, the phase noise tolerance could be improved simply by lowering N. The implemented carrier recovery algorithm is compatible with all kinds of equalizers for polarization control, chromatic dispersion (CD) and polarization mode dispersion (PMD).

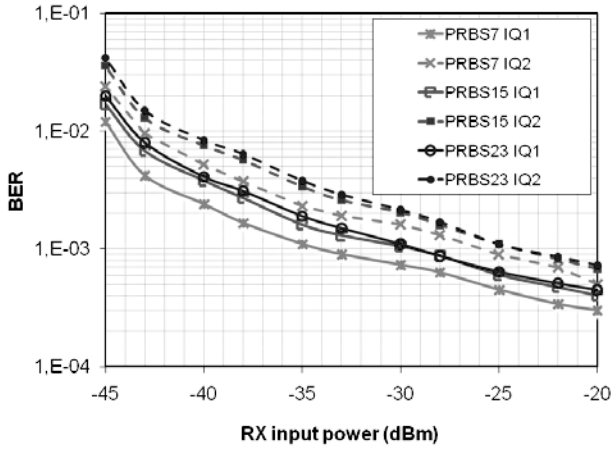

Fig. 12 Measured BERs of 16-QAM bits 1 and 2, each averaged over I&Q, vs. optical power at preamplifier input. Fiber length was 1.6 km.

6. Conclusions

A 2.5 Gb/s realtime transmission of 16-QAM with coherent detection and digital phase estimation and data recovery was presented. The averaged BER results reached the FEC threshold for a receiver input power below −30 dBm.

Acknowledgments

We thank the Deutsche Forschungsgemeinschaft (DFG) for supporting this work.

References

[1] T. Pfau, S. Hoffmann, R. Peveling, S. Bhandare, S.K. Ibrahim, O. Adamczyk, M. Porrmann, R. Noé, and Y. Achiam, "First real-time data recovery for synchronous QPSK transmission with standard DFB lasers," IEEE Photonic Technol. Lett., vol.18, no.18, pp.1907–1909, 2006.

[2] H. Sun, K. Wu, and K. Roberts, "Real-time measurements of a 40 Gb/s coherent system," Opt. Express, vol.16, pp.873–879, 2008.

[3] R. Noé, U. Rückert, S. Hoffmann, R. Peveling, T. Pfau, M. El-Darawy, and A. Al-Bermani, "Real-time implementation of digital coherent detection," Proc. European Conference on Optical Communication (ECOC2009), Tu5.4.3, Vienna, Austria, Sept. 2009.

[4] L. Molle, M. Seimetz, D. Gross, R. Freund, and M. Rohde, "Polarization multiplexed 20 gbaud square 16QAM long-haul transmission over 1120 km using EDFA amplification," We 8.4.4, ECOC 2009, Vienna, Austria, Sept. 2009.

[5] A. Gnauck and P. Winzer, "10 × 112-Gb/s PDM 16-QAM transmission over 1022 km of SSMF with a spectral efficiency of 4.1 b/s/Hz and no optical filtering," We 8.4.4, ECOC 2009, Vienna, Austria, Sept. 2009.

[6] Y. Mori, C. Zhang, M. Usui, K. Igarashi, K. Katoh, and K. Kikuchi, "200-km transmission of 100-Gbit/s 32-QAM dual-polarization signals using a digital coherent receiver," We 8.4.6, ECOC 2009, Vienna, Austria, Sept. 2009.

[7] T. Kawanishi, T. Sakamoto, and A. Chiba, "Integrated lithium niobate mach-zehnder interferometers for advanced modulation formats," IEICE Trans. Electron., vol.E92-C, no.7, pp.915–921, July 2009.

[8] I. Fatadin, D. Ives, and S. Savory, "Blind equalization and carrier phase recovery in a 16-QAM optical coherent system," J. Lightwave Technol., vol.27, no.15, pp.3042–3049, 2009.

[9] P. Winzer, H. Gnauk, S. Chandrasekhar, S. Draving, J. Evangelista, and B. Zhu, "Generation and 1,200-km transmission of 448-Gb/s ETDM 56-Gbaud PDM 16-QAM using a single I/Q modulator," Europ. Conf. on Optical Comm. (ECOC), paper PD2.2, 2010.

[10] A. Sano, T. Kobayashi, A. Matsuura, S. Yamamoto, S. Yamanaka, E. Yoshida, Y. Miyamoto, M. Matsui, M. Mizoguchi, and T. Mizuno, "100 × 120-Gb/s PDM 64-QAM transmission over 160 km using linewidth-tolerant pilotless digital coherent detection," Europ. Conf. on Optical Comm. (ECOC), paper PD2.4, 2010.

[11] T. Pfau, R. Peveling, V. Herath, S. Hoffmann, C. Wördehoff, O. Adamczyk, M. Porrmann, and R. Noé, "Towards real-time implementation of coherent optical communication," Proc. OFC/NFOEC 2009, invited paper, OThJ4, San Diego, CA, USA, March 2009.

[12] M. Nakamura, Y. Kamio, and T. Miyazaki, "Real-time 40-Gbit/s 16-QAM self-homodyne using a polarization-multiplexed pilot-carrier," IEEE/LEOS Summer Topical Meetings, 2008.

[13] T. Pfau, S. Hoffmann, and R. Noé, "Hardware-efficient coherent digital receiver concept with feedforward carrier recovery for M-QAM constellations," Lightwave Technol., vol.27, no.8, pp.989–999, 2009.

[14] M. Seimetz, "Multi-format transmitters for coherent optical M-PSK and M-QAM transmission," Proc. ICTON, Th.B1.5. Barcelona, 2005.

[15] T. Sakamoto, A. Chiba, and T. Kawanishi, "50-km SMF transmission of 50-Gb/s 16 QAM generated by quad-parallel MZM," Proc. European Conference on Optical Communication (ECOC), Tu.1.E.3, 2008.

[16] S. Savory, "Digital coherent optical receivers: Algorithms and subsystems," IEEE J. Sel. Top. Quantum Electron., vol.16, no.5, 2010.

[17] S. Hoffmann, T. Pfau, O. Adamczyk, C. Wördehoff, R. Peveling, M. Porrmann, R. Noé, and S. Bhandare, "Frequency estimation and compensation for coherent QPSK transmission with DFB lasers," Coherent Optical Technologies and Applications, Optical Society of America, paper CWB4, 2008.

[18] S. Hoffmann, T. Pfau, O. Adamczyk, R. Peveling, M. Porrmann, and R. Noé, "Hardware-efficient and phase noise tolerant digital synchronous QPSK receiver concept," Proc. COTA 2006, Paper CThC6, 2006.

[19] F. Rice, M. Rice, and B. Cowley, "A new algorithm for 16-QAM carrier phase estimation using QPSK partitioning," Digit. Signal Process., vol.12, no.1, pp.77–86, 2002.

[20] I. Fatadin, D. Ives, and S. Savory, "Laser linewidth tolerance for 16-QAM coherent optical systems using QPSK partitioning," IEEE Photonics Technol. Lett., vol.22, no.9, pp.631–633, 2010.

[21] T. Pfau and R. Noé, "Phase-noise-tolerant two-stage carrier recovery concept for higher order QAM formats," IEEE J. Sel. Top. Quantum Electron., vol.16, no.5, pp.1210–1216, 2010.

[22] X. Zhou, "An improved feed-forward carrier recovery algorithm for coherent receivers with M-QAM modulation format," IEEE Photonics Technol. Lett., vol.22, no.14, pp.1051–1053, 2010.

[23] R. Noé, "PLL-free synchronous QPSK polarization multiplex/diversity receiver concept with digital I&Q baseband processing," IEEE Photonics Technol. Lett., vol.17, no.4, pp.887–889, 2005.

[24] W. Weber, "Differential encoding for multiple amplitude and phase shift keying systems," IEEE Trans. Commun., vol.CON-26, no.3, pp.385–391, March 1978.

[25] J. Volder, "The CORDIC trigonometric computing technique," IRE Trans. Electronic Computers, vol.EC-8, no.3, pp.330–334, 1959.

Ali Al-Bermani was born in Baghdad, Iraq, in 1980. He received the B.Sc. and M.Sc. degrees in electronic and communications engineering/modern communication from Al-Nahrain University, Iraq, in 2001 and 2004, respectively. After graduation, he joined the Ministry of Electricity/Communication Department, Baghdad. In 2006 he joined Al-Nahrain University/college of information engineering as a lecturer. In 2008, he was granted a scholarship from the German Academic Exchange Service (DAAD) for Ph.D. studies at the University of Paderborn, Germany. He joined the working group "Optical Communication and High Frequency Engineering" of Prof. Noé where he is currently focusing on the development and implementation of a realtime coherent 16-QAM transmission system.

Christian Wördehoff was born in Büren, Germany, in 1978. He received the Dipl.-Ing. degree in Electrical Engineering from the University of Paderborn in 2007. From 2007 to 2010 he was with the Heinz Nixdorf Institute, department of System and Circuit Technology, University of Paderborn. Currently he is with the research group "Cognitronics and Sensor Systems", CITEC, Bielefeld University. His research interests include resource efficient microelectronic realizations of digital communication systems and real-time prototyping platforms. Christian Wördehoff is reviewer for the IEEE Photonics Technology Letters.

Sebastian Hoffmann was born in Bielefeld, Germany, in 1969. He received the Dipl.-Ing., Dipl.- Wirt.-Ing., and Dr.-Ing. degrees from the University of Paderborn, Paderborn, Germany, in 1997, 2000, and 2008, respectively. From 1988 to 1992, he was on vocational training as a Power Electronics Technician at Miele & Cie. KG, Bielefeld, Germany. Then, he studied electrical engineering in Paderborn, Germany, and Waterloo, ON, Canada. He is currently as a Postdoctoral Researcher with the Optical Communication and High-Frequency Engineering, University of Paderborn. He has contributed to various projects, including microelectronics, high-frequency engineering, and optical communication. He is also working as a part-time lecturer at the University of Applied Science in Bielefeld. Dr. Hoffmann is a reviewer for the IEEE Photonics Technology Letters and the IEEE Journal of Lightwave Technology.

Timo Pfau was born in Stuttgart, Germany, in 1979. He received the Dipl.-Ing. degree in electrical engineering and information technology from the University of Stuttgart, Stuttgart, in 2004, and the Dr.-Ing. degree (with highest honors) in electrical engineering from the University of Paderborn, Paderborn, Germany, in 2009. After graduation, he was granted a scholarship from the International Graduate School "Dynamic Intelligent Systems," University of Paderborn. Since June 2009, he has been a member of the Technical Staff at Bell Laboratories, Alcatel-Lucent, Murray Hill, NJ. His current research interests include algorithm development for coherent optical receivers with digital signal processing and real-time implementation of coherent optical transmission systems using advanced modulation formats.

Ulrich Rückert received the Diploma degree in Computer Science and a Dr.-Ing. degree in Electrical Engineering from the University of Dortmund, Germany, in 1984 and 1989, respectively. From 1985 to 1992 he worked on microelectronic implementation of neural networks at the Faculty of Electrical Engineering (University of Dortmund). From 1993 to 1994 he was Professor at the Technical University of Hamburg-Harburg, Germany, heading a research group on Microelectronics. In 1995 he joined the Heinz Nixdorf Institute at the University of Paderborn, Germany. As a Full Professor he was head of the research group "System and Circuit Technology". The group was working on innovative circuit design and development of microelectronic systems for massive-parallel and resource-efficient information processing. Since 2001 he is Adjunct Professor of the Faculty of Information Technology, Queensland University of Technology, Brisbane, Australia. Since 2009 he is Professor at Bielefeld University, Germany. His research group "Cognitronics and Sensor Systems" is member of the "Cognitive Interaction Technology – Cluster of Excellence". His main research interests are now bio-inspired architectures for Nanotechnologies and cognitive robotics. He has authored or coauthored more than 250 journal and conference publications. Together with R. Noé, he received the Innovation Award 2008 of North Rhine-Westphalia in category innovation.

Reinhold Noé was born in Darmstadt, Germany, in 1960. He received the Dipl.-Ing. and Dr.-Ing. degrees in electrical engineering from the Technische Universität München, Munich, Germany, in 1984 and 1987, respectively. He realized the first endless polarization control systems. He was a Postdoctoral Fellow with Bellcore, Red Bank, NJ, where he worked on coherent optical systems. In 1988, he joined Siemens Research Laboratories, Munich. In 1992, he implemented the first synchronous optical phase-shift keying (PSK) transmission with normal distributed feedback (DFB) lasers. Since 1992, he has been the Chair of the Optical Communication and High-Frequency Engineering, University of Paderborn, Paderborn, Germany. His current research interests include high-speed endless optical polarization control and real-time synchronous QPSK and QAM transmission. He has authored or coauthored more than 240 journal and conference publications. Together with U. Rückert, he received the Innovation Award 2008 of North Rhine-Westphalia in category innovation.